On the Local Structure in Ordered and Disordered *Closo*-Hydroborate Solid Electrolytes

Paul Till[a], Ryo Asakura[b], Arndt Remhof[b], Wolfgang G. Zeier*[a,c]

[a] *Institute of Inorganic and Analytical Chemistry, University of Münster, Corrensstraße 28/30, D-48149 Münster, Germany.*

[b] *Materials for Energy Conversion, Empa, Swiss Federal Laboratories for Materials Science and Technology, 8600 Dübendorf, Switzerland.*

[c] *Institut für Energie- und Klimaforschung (IEK), IEK-12: Helmholtz-Institut Münster, Forschungszentrum Jülich, 48149 Münster, Germany.*

Abstract

Na^+ *closo*-hydroborates are a heavily researched solid electrolyte class for applications in all-solid-state Na batteries. The structural characterization of these materials is notoriously challenging due to the elements involved and the fast rotational motion of hydroborate cages. The average structures obtained by Bragg diffraction have numerous atomic positions with low occupancies, complicating the determination of actual atom-atom distances. Total average scattering and derived pair distribution functions display atom-atom distances in real space, providing additional structure information to the average crystal structure. In this work, we present the pair distribution functions of the five different Na^+ *closo*-hydroborates: $Na_2B_{10}H_{10}$, $Na_2B_{12}H_{12}$ and $NaCB_{11}H_{12}$, and the mixtures of 1:1 $Na_2B_{12}H_{12}$:$Na_2B_{10}H_{10}$ and 2:1 $NaCB_{11}H_{12}$:$Na_2B_{12}H_{12}$. All pair distribution functions show a fast decay of peak height with increasing atom-atom distance on the local scale, suggesting a low correlation of atom motions between borate cages, as observed in various other molecular crystals. The combination of Bragg diffraction, showing the average ordering of *closo*-hydroborate cages, and pair distribution function analysis, providing local atom-atom distances, is a useful tool to develop a deeper understanding of the *closo*-hydroborates and also of other plastic crystals.

1. Introduction

Na^+ *closo*-hydroborates have recently garnered increasing research interest as solid electrolytes for all-solid-state battery applications.[1–4] This solid electrolyte class combines several desirable properties for the implementation in solid-state batteries, such as high room-temperature ionic conductivity, low density, good mechanical processability and low toxicity.[5,6] Especially the reports of 3 V and 4 V all-solid-state Na batteries employing Na^+ hydroborate solid electrolytes have highlighted the relevance and applicability of these materials for energy storage technologies.[7,8]

Structural characterization of Na^+ *closo*-hydroborates, however, has been notoriously challenging since single crystals could hardly be obtained. Hence, structure solving has been carried out by combined powder diffraction techniques and computational structure calculation.[9,10] Small X-ray scattering form factors of B and H atoms further impede structure solving by X-ray diffraction. Cage orientations were reported with high uncertainty and neutron diffraction experiments were carried out at low temperatures on $Na_2B_{10}D_{10}$ for a more precise structure description;[11] nevertheless, neutron experiments themselves are highly challenging with the high absorption cross-section of natural boron.

Furthermore, the high-conductivity phases that are interesting for battery applications exhibit a high degree of orientational disorder, stemming from the rotations of *closo*-hydroborate anions and the high mobility of the jumping Na^+ ions.[12–14] In these phases, Bragg diffraction can only provide limited information on actual atom-atom distances, because averaged diffraction patterns are a sample over various local configurations, projected into one unit cell. The resulting structural models usually have many partially occupied atom positions, which makes it challenging to interpret the actual crystal structure, to determine atom-atom distances and ultimately to correlate the structure-transport properties, if not impossible.

Pair distribution functions $D(r)$ obtained from total X-ray diffraction measurements are histograms of atom-atom distances and can thereby provide structural information on the local scale. These local atom-atom distances can be also determined in solids with a high degree of dynamic disorder.[15–19] To evaluate the capabilities of total-scattering-based structure characterization for Na^+ *closo*-hydroborates, total X-ray scattering experiments were performed for five *closo*-hydroborates, namely $Na_2B_{10}H_{10}$, $Na_2B_{12}H_{12}$, $NaCB_{11}H_{12}$, and compounds with mixed anions of 1:1 $Na_2(B_{12}H_{12})$:$Na_2(B_{10}H_{10})$ (= $Na_4(B_{12}H_{12})(B_{10}H_{10})$) and 2:1

$NaCB_{11}H_{12}$:$Na_2B_{12}H_{12}$ (= $Na_4(CB_{11}H_{12})_2(B_{12}H_{12})$). The *closo*-hydroborate cages of $Na_2B_{10}H_{10}$ and $Na_2B_{12}H_{12}$ are reported to crystalize in the ordered structures in space group $P2_1/c$ or the transform $P2_1/n$.[9,11] As observed by ^{1}H-NMR spectroscopy, the cages are also rotating at room temperature,[20,21] but jumps occur between the same set of Wyckoff positions and thus do not lead to disorder, which would be observable by diffraction techniques. Further, $NaCB_{11}H_{12}$ is an ordered structure at room temperature (space group $Pca2_1$).[22] Compared to $Na_2B_{12}H_{12}$ and $Na_2B_{10}H_{10}$ the cage rotation frequencies at room temperature are higher, which is also reflected by a lower transition temperature to the disordered phase.[21–23] The two mixed compounds $Na_4(B_{12}H_{12})(B_{10}H_{10})$ and $Na_4(CB_{11}H_{12})_2(B_{12}H_{12})$ were reported to crystallize in the disordered polymorphs at room temperature, and hence the cages have high rotation frequencies.[5,14] A random distribution of the different cages introduces additional disorder into the structure.

In this work, we will show that the measured pair distribution functions $D(r)$ reveal similar short-range atom-atom distances and that the peak height decreases fast with the interatomic distance r in all compounds, irrespective of composition. Simulations of pair distribution functions from known ordered structures are carried out to assign specific atom-atom distances, and thereby obtain a better understanding for the decreasing peak height with increasing r. The learnings from the ordered structures are applied to the disordered phases and enable identification of local atom to atom distances. Eventually, the observed diffraction characteristics on the average and local scale are discussed in the context of a plastic crystal classification in the case of the disordered Na^+ *closo*-hydroborates.

2. Methods

Synthesis. $Na_2B_{10}H_{10}$, $Na_2B_{12}H_{12}$, and $NaCB_{11}H_{12}$ were purchased from Katchem. $Na_2B_{12}H_{12}$ was used as received, while $Na_2B_{10}H_{10}$ and $NaCB_{11}H_{12}$ were dried under dynamic vacuum ($<10^{-3}$ mbar) at 180 °C and 240 °C for 6 h and 12 h, respectively. $Na_4(B_{12}H_{12})(B_{10}H_{10})$ was synthesized from an equimolar mixture of $Na_2B_{12}H_{12}$ and dried $Na_2B_{10}H_{10}$ by high-energy ball milling using a Spex 8000M shaker mill with a ball-to-sample mass ratio of 10:1 for three times 15 min with 5 min breaks to avoid overheating.[7,12] Subsequently, the sample was heat treated under vacuum ($<10^{-3}$ mbar) at 270 °C for 12 h to fully react and crystalize the compound. $Na_4(CB_{11}H_{12})_2(B_{12}H_{12})$ was prepared by a 2:1 molar mixture of dried $NaCB_{11}H_{12}$ and $Na_2B_{12}H_{12}$ by high-energy ball milling using a Spex 8000M shaker mill with a ball-to-sample mass ratio of 40:1 for four times 15 min with 5 min breaks.[8,14] All compounds were stored and handled in an argon-filled glovebox (MBraun, O_2 and H_2O levels <0.1 ppm).

X-ray total scattering experiments. Samples were filled into quartz capillaries (1 mm outer diameter) under argon atmosphere and sealed with vacuum grease and Loctite glue. X-ray total scattering experiments were carried out at the Diamond light source I15-1 beamline. A wavelength of 0.161669 Å and PerkinElmer area detector with a sample to detector distance of 200 mm was used to collect total scattering data for PDF calculation. A second Perkin Elmer detector was positioned 850 mm away from the sample for the collection of higher resolution Bragg data. Scattering data were acquired at room temperature in a 2θ range 0° – 25° with a step size of 0.01°. Total measurement time was 30 minutes for $Na_2B_{10}H_{10}$, $Na_2B_{12}H_{12}$, $NaCB_{12}H_{12}$ and $Na_4(CB_{11}H_{12})_2(B_{12}H_{12})$, and 20 minutes for $Na_4(B_{12}H_{12})(B_{10}H_{10})$. An empty capillary measurement was carried out for background subtraction. The GudrunX program[24] was used for background correction, normalization and Fourier transform with a maximum scattering vector Q_{max} of 23 $Å^{-1}$. The PDF $D(r)$ was obtained as defined by Keen.[25]
Simulation of the pair distribution functions was carried out with the PDFgui program[26], using the reported structure of $Na_2B_{12}H_{12}$.[9] Lattice parameters for the simulation were adjusted to those determined from Pawley fitting. Thermal displacement parameters were reduced to 0.005 $Å^2$ for all atoms for better identification of single atom-atom distances.

Bragg data analyses. Pawley fits were carried out for space group confirmation and determination of lattice parameters using the TOPAS V6 Academic software (Coelho Software, Brisbane, Australia).[27] For the diffraction pattern fitting, the background was modelled by manually placed and fixed background points. The peak shape was described by a Thomson-Cox-Hastings pseudo-Voigt function and asymmetry was modelled by a simple axial model.

3. Results and Discussion

Structural information in single cluster compounds. The obtained Bragg diffraction data and the corresponding pair distribution functions of $Na_2B_{10}H_{10}$, $Na_2B_{12}H_{12}$ and $NaCB_{11}H_{12}$ are shown in Figure 1. All three compounds were found to crystallize in their ordered crystal structure and lattice parameters derived from Pawley fits are provided in the Supporting Information. Due to the limited structural information found in the diffraction patterns, Rietveld refinements are not possible.

The pair distribution functions of all three compounds are similar with respect to their low r region, where two sharp peaks are observed. For $r > 4$ Å, the peak height decreases significantly, compared to the $r < 4$ Å region. This decrease is especially pronounced in $NaCB_{11}H_{12}$ where the $D(r)$ is almost featureless for larger r. Even though the peaks are broad at high r and have a

low height, the presence of periodic, almost oscillation like peaks clearly alludes to the long-range order on the local scale. Such a persisting long-range order with a low peak height is known for the pair distribution functions of molecular crystals.[28,29] To explain the origin of the height decay with increasing *r* in the Na^+ *closo*-hydroborates, the measured *D*(*r*) peaks are assigned to atom-atom distances.

For this assignment, pair distribution functions were simulated for the reported ordered structures[9,11] of $Na_2B_{12}H_{12}$ and $Na_2B_{10}H_{10}$, with lattice parameters adjusted to those obtained from Pawley refinements. The simulations were carried out to yield partial pair distribution functions, which only contain information on specified atom-atom distances. For examples, the simulated partial B-B pair distribution functions contain only those pair correlations which arise from B-B distances. For $Na_2B_{12}H_{12}$ and $Na_2B_{10}H_{10}$, similar results were obtained, so that the findings for $Na_2B_{12}H_{12}$ will be discussed exemplarily further down below, and results obtained for $Na_2B_{10}H_{10}$ are added in the Supporting Information for completeness.

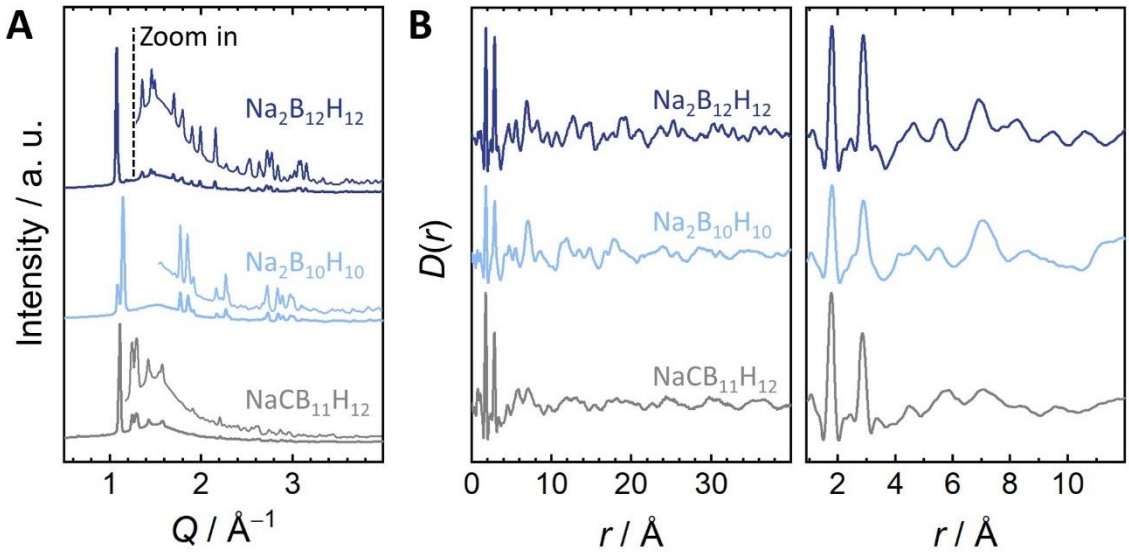

Figure 1: a) Bragg diffractograms and zoom in on higher Q reflections of $Na_2B_{12}H_{12}$, $Na_2B_{10}H_{10}$ and $NaCB_{11}H_{12}$. b) Pair distribution functions D(r) as determined from total synchrotron X-ray scattering experiments. At low r, two high-intensity peaks are found for all compounds. All further peaks are significantly less intense, and the D(r) of $NaCB_{11}H_{12}$ is almost flat for r > 10 Å. The magnification in the right panel shows the similar low r features of all three compounds.

As seen in Figure 2, many of the features in the measured pair distribution function of $Na_2B_{12}H_{12}$ can be explained by pair interactions arising from B-B distances. Two distinctly different regions can be defined. The intra-cage region up to 4 Å incorporates the nearest and next-nearest neighbor B-B distances within one cage, resulting in sharp peaks. The inter-cage region for *r* > 4 Å captures all B-B distances between different cages and the resulting peaks

are broad and have a low height. Both regions are highlighted in Figure 2 and the difference between them can be explained as follows:

The counting statistics in both regions are significantly different. In the intra-cage region, a high number of the same B-B distances, namely the nearest neighbor and next-nearest neighbor B-B distances is found, due to the high symmetry of the cage arrangement and the distinct bond length dictated by covalent bonding interactions. In the inter-cage region, on the other hand, a large spread in B-B distances is observed, with a lower number of the same B-B distance per unit volume, compared to the intra-cage region. Consequently, the peaks in the observed inter-cage region are an overlap of various B-B pair peaks of low height, resulting in overall broad peaks.

Additionally, correlated motions of atoms influence the $D(r)$ peak width.[30] Strong covalent bonding interactions act between the B atoms within the *closo*-borate cages, leading to highly correlated motions and consequently sharp peaks in the intra-cage region. In the inter-cage region on the other hand, these strong interactions are not present anymore, so that the B atom motions between cages are only weakly correlated, i.e., the vibrational coupling between cages is low, which leads to broad peaks. The interactions between cages, are in fact so weak, that rotation motions are possible, also in the ordered phases, as observed by ^{1}H NMR.[20,21]

These differences in peak height and width between intra-cage and inter-cage regions are known for various molecular solids.[31] Similar to the *closo*-hydroborates, C_{60} fullerenes for example show a flattening of the $D(r)$ once r is larger than the intra-cage region.[32] Interestingly enough, the C_{60} buckyballs were reported to rotate at room temperature.[33]

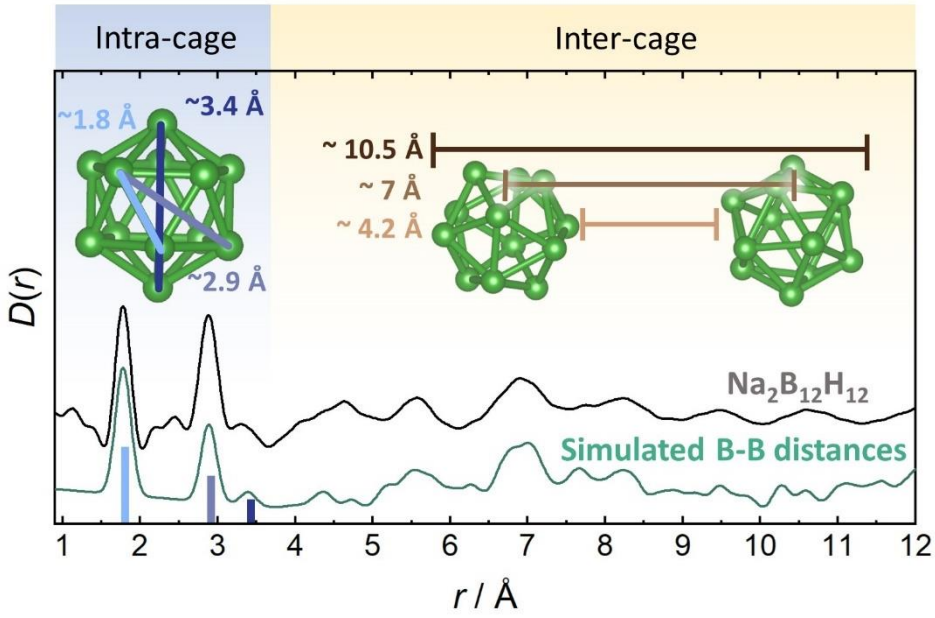

Figure 2: Measured D(r) of $Na_2B_{12}H_{12}$ and the simulated partial D(r) that arises from B-B distances only. The published structure from reference 9 with adjusted lattice parameters was used for the simulation. In the low r region, D(r) peaks correspond to intra-cage B-B distances. For r > 4 Å, inter-cage B-B distances are observed. Since various inter-cage B-B distances are found, the D(r) is broad. The feature around 7 Å corresponds to the center of mass distance of neighboring cages. The largest B-B distances of neighboring cages are found around ~10.5 Å.

For $Na_2B_{12}H_{12}$, Her and co-workers describe the Na^+ coordination by hydroborate cages as tetrahedral, with Na^+ being positioned close to one triangular plane.[9] The calculated partial Na^+-B pair distribution function, shown in Figure 3a, has its first peak from ~2.8 Å to 3.5 Å, corresponding to Na^+ surrounded by nine B atoms within the tetragonal plane, as shown in the inset. The peak around 4 Å then corresponds to pair interactions of Na^+ and B atoms located at the hydroborate cage of the coordinating tetrahedron that is located further away from Na^+. This peak also overlaps with peaks arising from Na^+-B distances within the triangular plane. While the first Na^+-B coordination sphere can be well-identified from the simulated pair distribution function, this is not possible for further coordination spheres. Since the hydroborate cages are spatially extended (i.e., $D(r)$ signals range from 2.8 Å up to 5.7 Å), Na^+-B peaks from the nearest neighbor cages overlap with regions of Na^+-B peaks from the next-nearest neighbor cages and so on. Therefore, a continuum of Na^+-B peaks is observed.

Distinct Na^+-Na^+ distances, on the other hand, can be clearly identified in the partial Na^+-Na^+ pair distribution function and groups of peaks are separated by sections with a flat partial pair distribution function, as shown in Figure 3b. Each *closo*-borate cage is surrounded by eight Na^+ ions, creating a network of edge sharing Na_8B_{12} polyhedra. Each Na^+ is surrounded by six other

Na^+ in an octahedral arrangement as shown in the inset in Figure 3b. Five of these Na^+ are closer to the central Na^+ (between 4.5 Å and 5.3 Å), giving rise to the first group of peaks in the partial Na^+-Na^+ pair distribution function. One Na^+ is located further away from the central Na^+ (6.7 Å) and the corresponding Na^+-Na^+ distance is located within the next group of peaks, as shown in Figure 3b. However, the peaks arising from Na^+-Na^+ distances are hardly observable in the measured $D(r)$ due to the low relative intensity. In this case, studying the partial Na^+-Na^+ pair distribution function is more helpful to visualize the Na^+-Na^+ distances in the published structure, than understanding the measured $D(r)$

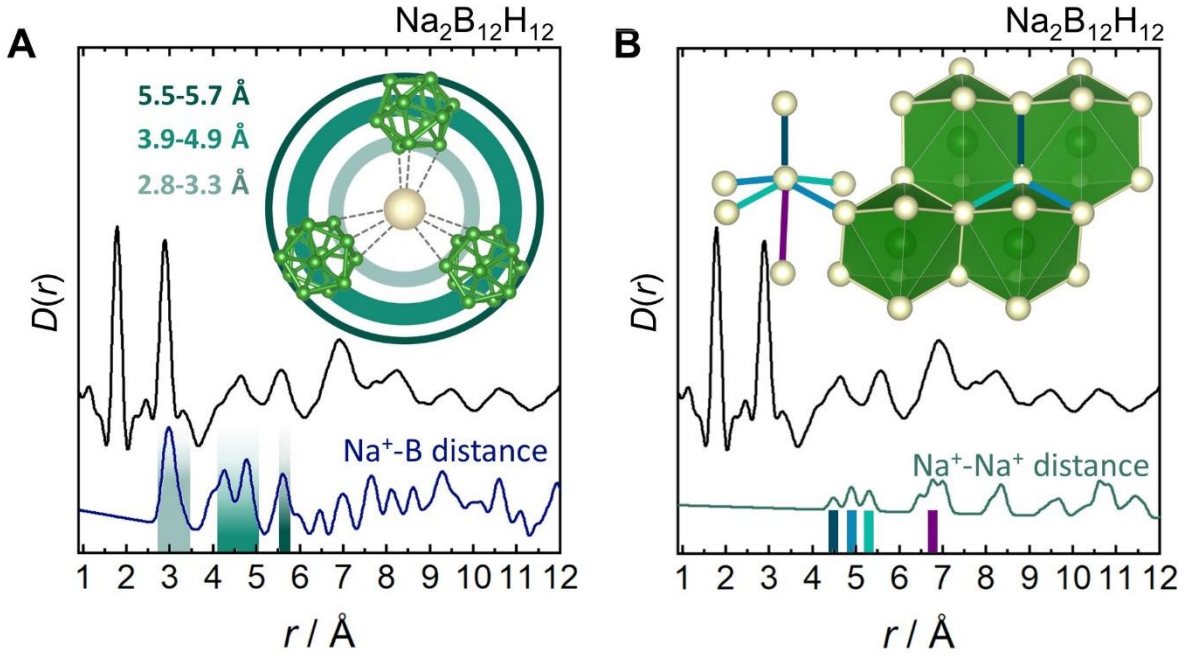

Figure 3: a) Measured D(r) of $Na_2B_{12}H_{12}$ compared to the simulated partial D(r) of Na^+-B distances. The most intense peak around 3 Å arises from the first B coordination sphere. Na^+-B distances of these nearest B cages extend up to 5.7 Å. Within this distance, two further hydroborate cages are found, which also contributes to the D(r) so that a continuum of Na^+-B peaks is observed. b) Measured D(r) of $Na_2B_{12}H_{12}$ compared to the simulated partial D(r) of Na^+-Na^+ distances. Eight Na^+ surround each borate cage. The cages were simplified by spheres, as shown in the inset. The coordination polyhedra are edge sharing. Na^+ is surrounded by other Na^+ octahedrally, resulting in five shorter and one longer Na^+-Na^+ distance.

Structural information of mixed *closo*-hydroborates with highly disordered structures. The stabilization of the disordered *closo*-hydroborate phases – which have a high conductivity necessary for battery applications – can be achieved in mixed-anion hydroborate compounds.[12,14,34] Collected Bragg data of $Na_4(B_{12}H_{12})(B_{10}H_{10})$ and $Na_4(CB_{11}H_{12})_2(B_{12}H_{12})$ are shown in Figure 4a. A Pawley fit (see Supporting Information) confirms the formation of the disordered face-centered phase in $Na_4(B_{12}H_{12})(B_{10}H_{10})$. Additional reflections also indicate the presence of unreacted $Na_2B_{10}H_{10}$ and $Na_2B_{12}H_{12}$ (see Figure S2). Phase identification of

$Na_4(CB_{11}H_{12})_2(B_{12}H_{12})$ was not possible due to broad reflections, most likely caused by strain in the crystallites that is induced through ball milling.[35]

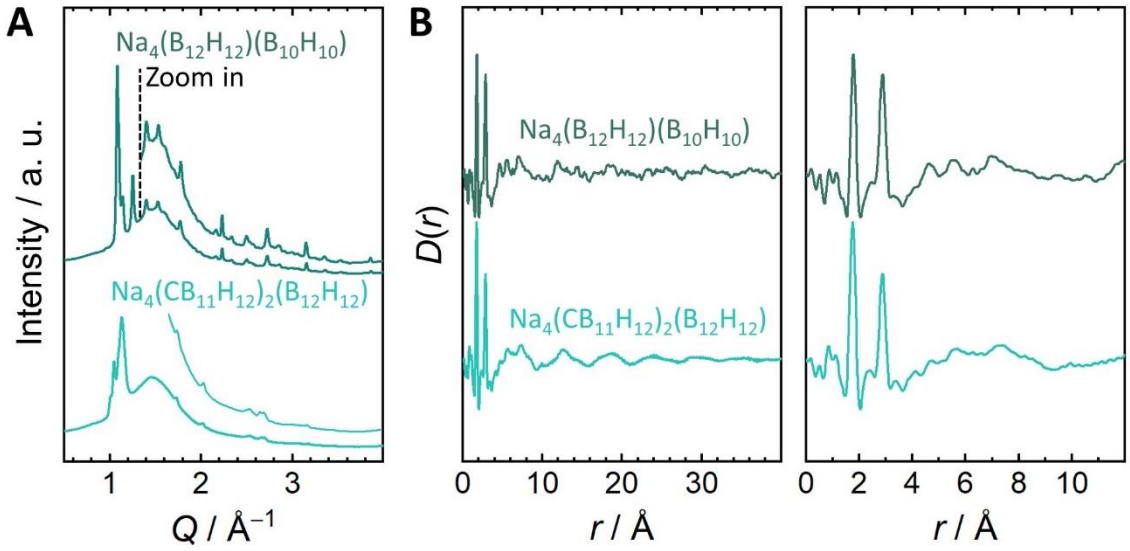

Figure 4:a) Bragg diffractograms and a zoom in on higher Q reflections of the mixed cage compounds $Na_4(B_{12}H_{12})(B_{10}H_{10})$ and $Na_4(CB_{11}H_{12})_2(B_{12}H_{12})$. b) Measured D(r) of both mixed compounds. The shown D(r) have similar features to the compounds with non-mixed cages, i.e., both D(r) have a high intensity at low r and a rapid intensity loss with increasing r. The magnification in the right panel shows that both compounds have similar low r features, despite the different cages.

The obtained pair distribution functions of the mixed-anion compounds $Na_4(B_{12}H_{12})(B_{10}H_{10})$ and $Na_4(CB_{11}H_{12})_2(B_{12}H_{12})$ are shown in Figure 4b. Similar to the compounds with just one cage-type, two sharp peaks at low *r* are observed. At higher *r* the pair distribution function is almost featureless and only a periodic pattern which is attributable to a long-range order of cages is seen. A comparison of all measured samples in the low *r* range in Figure S5 shows the same low *r* atom-atom distances for all pair distribution functions. Knowing that the low *r* peaks correspond to the nearest neighbor B-B and Na^+-B distances from the ordered phases, we can conclude that similar local atom-atom distances are present in disordered phases as well. Such information is hardly obtained from Bragg diffraction, highlighting the knowledge gain from pair distribution function analyses in terms of local structural environments for short interatomic distances. On the other hand, in these compounds pair distribution function analyses can barely provide information beyond the short-range bond distances, because structure modeling using higher *r* ranges may not deliver accurate structure descriptions due to the low peak height and broad, featureless *D*(*r*) at high *r*. Such information, however, can be well obtained from Bragg diffraction, showing that the combination of both diffraction techniques

is a helpful approach to obtain additional information for structure description in these disordered phases.

Discussion of local versus average scale in these *closo*-hydroborates. As determined from simulated partial $D(r)$, the measured $D(r)$ is largely determined by the B-B distances (compare Figure S6 and S7), so that the pair distribution function can be distinguished into an intra-cage region with sharp peaks an inter-cage region with broad features and a low peak height. The reason for the observed peak height decay going from the intra-cage to the inter-cage region is significantly different from the reason of a peak height decay in amorphous solids, where the asymmetric arrangement of atoms or polyanionic units leads to a low coherence length. Additionally, even if the peaks are of low height at high r periodic features still remain in the *closo*-hydroborates, indicative of long-range order. Therefore, while the $D(r)$ may be reminiscent of a glass on a local scale at first glance, the origin is different and these *closo*-hydroborates are clearly not amorphous phases. As a consequence, the average-scale Bragg diffraction patterns are in no contradiction to the rapid drop of the peak height. On the average scale, the hydroborate cages are arranged periodically and produce the Bragg diffraction patterns. On the local scale, on the other hand, atom-atom motion correlations and counting statistics are changed drastically once B-B distances in the inter-cage regions are considered, causing the observed peak height decay. These effects are even more pronounced in the mixed-cage compounds, due to the high reorientational cage disorder resulting in an almost featureless $D(r)$ at high r.

As mentioned in earlier publications, the disordered phases of the *closo*-hydroborates were classified as plastic crystalline phases. Plastic crystals are mesophases between a liquid state and a solid state and show high rotational dynamics of the constituting molecules or polyions.[32,36,37] While Bragg diffraction captures the periodic arrangement of rotating molecules or ions, which gives rise to the solid nature of the plastic crystal, the pair distribution function alludes to the fast loss of local correlation that is found in liquids.[38,39] This combination of average-scale diffraction patterns and almost featureless pair distribution functions at higher r was reported for various plastic crystals.[16,40,41] Thus, it is convenient to find the corresponding mesophasic diffraction characteristics also in the rotationally disordered *closo*-hydroborates, further corroborating the classification of these materials as plastic crystals.

In the case presented here, combined Bragg diffraction and pair distribution function analyses helped to develop a deeper understanding of the *closo*-hydroborate structures and highlight the plastic-crystalline characteristics of the disordered phases in this material class. The

complementary information obtained from both diffraction techniques, is not only suitable to elucidate the structures of the *closo*-hydroborates, but of plastic crystals in general.

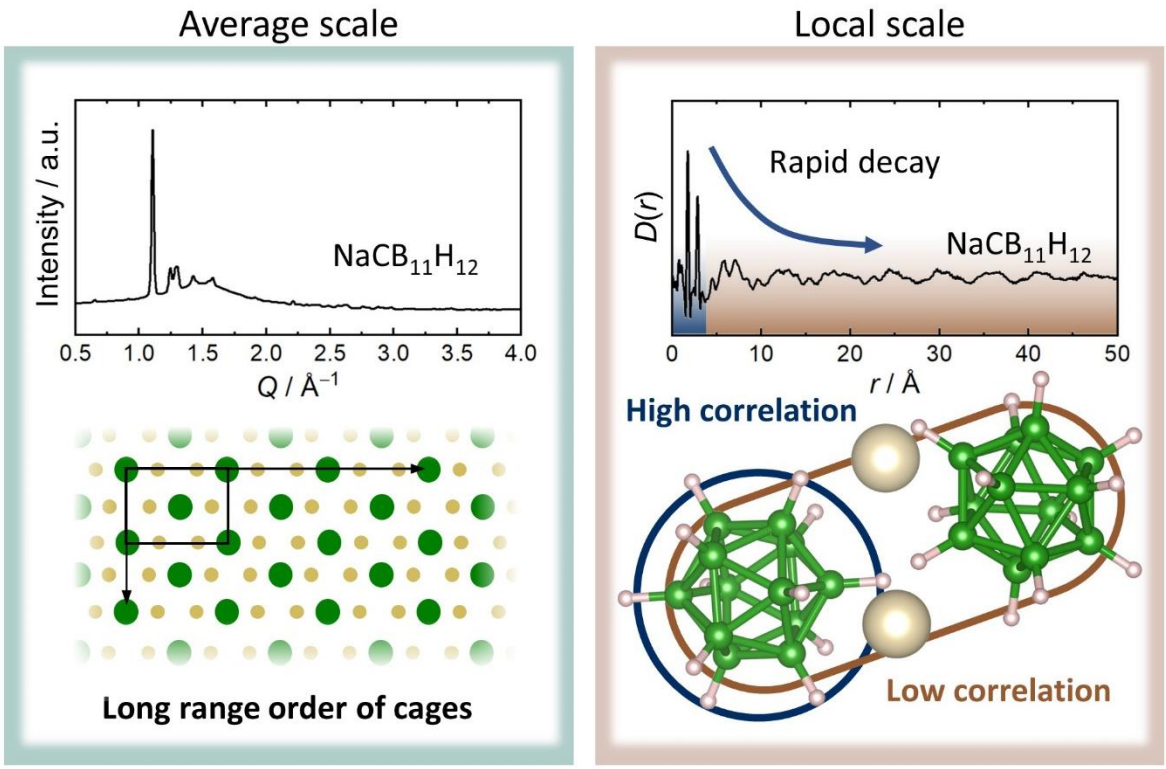

Figure 5: Schematic representation of effects present on the average and locale scale. Left: Bragg patterns arise from the periodic arrangement of hydroborate cages on the average scale. Right: The measured pair distribution function decays quickly, once B-B distances in the inter-cage region are considered, due to different counting statistics compared to the intra-cage region and the low motion-correlation between B atoms residing at different borate cages.

4. Conclusions

In this work, the local structure of five Na^+ *closo*-hydroborate compounds was assessed by pair distribution function analyses. The obtained pair distribution functions are characterized by sharp peaks at low *r* and a peak height decrease with increasing *r*. As derived from atom-specific simulated pair distribution functions, this decrease is caused by the cage structure of the *closo*-borates. In the low *r* inter-cage region, high counting statistics and high correlation of B motions lead to sharp peaks. In the higher r inter-cage region, a large variety of different B-B distances are found and B motions of atoms residing at different cages are only weakly correlated, which results in broad peaks with low height. Thus, the fast height decay with increasing *r*, is not contradicting the Bragg reflections arising from periodically ordered hydroborate cages, which is a common observation in plastic crystals. Combining the

complementary information from the local and average scale can help to develop a deeper understanding of *closo*-hydroborate structures and plastic crystals in general.

AUTHOR INFORMATION

Corresponding Authors

*wzeier@uni-muenster.de;

Notes

The authors declare no competing financial interests.

ASSOCIATED CONTENT

Supporting information

The Supporting Information contains Pawley fits and derived lattice parameters of all samples. All simulated atom-atom specific *D(r)* are compared. A comparison of all measured *D(r)* is shown.

ACKNOWLEDGEMENTS

The research as supported by the Deutsche Forschungsgemeinschaft (DFG) under grant number ZE 1010/6-1. This work was carried out with the support of Diamond Light Source, instrument I11 (Reference No. CY26379). The authors would also like to thank the Beamline-Scientist Dr Philip Chater for the collection and processing of total scattering data.

References

(1) Duchêne, L.; Remhof, A.; Hagemann, H.; Battaglia, C. Status and Prospects of Hydroborate Electrolytes for All-Solid-State Batteries. *Energy Storage Mater.* **2020**, *25*, 782–794. https://doi.org/10.1016/j.ensm.2019.08.032.

(2) Asakura, R.; Remhof, A.; Battaglia, C. Hydroborate-Based Solid Electrolytes for All-Solid-State Batteries; Gupta, R. K., Eds; *ACS Symposium Series*, **2022**, 1413, 353-393. https://doi.org/10.1021/bk-2022-1413.ch014.

(3) Brighi, M.; Murgia, F.; Černý, R. Closo-Hydroborate Sodium Salts as an Emerging Class of Room-Temperature Solid Electrolytes. *Cell Reports Phys. Sci.* **2020**, *1*, 100217. https://doi.org/10.1016/j.xcrp.2020.100217.

(4) Cuan, J.; Zhou, Y.; Zhou, T.; Ling, S.; Rui, K.; Guo, Z.; Liu, H.; Yu, X. Borohydride-Scaffolded Li/Na/Mg Fast Ionic Conductors for Promising Solid-State Electrolytes. *Adv. Mater.* **2019**, *31*, 1803533. https://doi.org/10.1002/adma.201803533.

(5) Duchêne, L.; Lunghammer, S.; Burankova, T.; Liao, W. C.; Embs, J. P.; Copéret, C.; Wilkening, H. M. R.; Remhof, A.; Hagemann, H.; Battaglia, C. Ionic Conduction Mechanism in the $Na_2(B_{12}H_{12})_{0.5}(B_{10}H_{10})_{0.5}$ Closo-Borate Solid-State Electrolyte: Interplay of Disorder and Ion-Ion Interactions. *Chem. Mater.* **2019**, *31*, 3449–3460. https://doi.org/10.1021/acs.chemmater.9b00610.

(6) Muetterties, E. L.; Balthis, J. H.; Chia, Y. T.; Knoth, W. H.; Miller, H. C. Chemistry of Boranes. VIII. Salts and Acids of $B_{10}H_{10}^{-2}$ and $B_{12}H_{12}^{-2}$. *Inorg. Chem.* **1964**, *3*, 444–451. https://doi.org/10.1021/ic50013a030.

(7) Duchêne, L.; Kühnel, R. S.; Stilp, E.; Cuervo Reyes, E.; Remhof, A.; Hagemann, H.; Battaglia, C. A Stable 3 v All-Solid-State Sodium-Ion Battery Based on a Closo-Borate Electrolyte. *Energy Environ. Sci.* **2017**, *10*, 2609–2615. https://doi.org/10.1039/c7ee02420g.

(8) Asakura, R.; Reber, D.; Duchêne, L.; Payandeh, S.; Remhof, A.; Hagemann, H.; Battaglia, C. 4 V Room-Temperature All-Solid-State Sodium Battery Enabled by a Passivating Cathode/Hydroborate Solid Electrolyte Interface. *Energy Environ. Sci.* **2020**, *13*, 5048–5058. https://doi.org/10.1039/d0ee01569e.

(9) Her, J.-H.; Zhou, W.; Stavila, V.; Brown, C. M.; Udovic, T. J. Role of Cation Size on the Structural Behavior of the Alkali-Metal Dodecahydro- Closo-Dodecaborates. *J. Phys. Chem. C* **2009**, *113*, 11187–11189. https://doi.org/10.1021/jp904980m.

(10) Hofmann, K.; Albert, B. Crystal Structures of $M_2[B_{10}H_{10}]$ (M = Na, K, Rb) via Real-Space Simulated Annealing Powder Techniques. *Z. Kristallogr.* **2005**, *220*, 142–146. https://doi.org/10.1524/zkri.220.2.142.59144.

(11) Wu, H.; Tang, W. S.; Zhou, W.; Stavila, V.; Rush, J. J.; Udovic, T. J. The Structure of Monoclinic $Na_2B_{10}H_{10}$: A Combined Diffraction, Spectroscopy, and Theoretical Approach. *CrystEngComm* **2015**, *17*, 3533–3540. https://doi.org/10.1039/c5ce00369e.

(12) Duchêne, L.; Kühnel, R. S.; Rentsch, D.; Remhof, A.; Hagemann, H.; Battaglia, C. A Highly Stable Sodium Solid-State Electrolyte Based on a Dodeca/Deca-Borate Equimolar Mixture. *Chem. Commun.* **2017**, *53*, 4195–4198.

https://doi.org/10.1039/c7cc00794a.

(13) Udovic, T. J.; Matsuo, M.; Tang, W. S.; Wu, H.; Stavila, V.; Soloninin, A. V; Skoryunov, R. V; Babanova, O. A.; Skripov, A. V; Rush, J. J.; et al Exceptional Superionic Conductivity in Disordered Sodium Decahydro- Closo -Decaborate. **2014**, 7622–7626. https://doi.org/10.1002/adma.201403157.

(14) Brighi, M.; Murgia, F.; Łodziana, Z.; Schouwink, P.; Wołczyk, A.; Černý, R. A Mixed Anion Hydroborate/Carba-Hydroborate as a Room Temperature Na-Ion Solid Electrolyte. *J. Power Sources* **2018**, *404*, 7–12. https://doi.org/10.1016/j.jpowsour.2018.09.085.

(15) Tsuchiya, Y.; Tamaki, S.; Waseda, Y. Structural Study of Superionic Phase of AgI. *J. Phys. C: Solid State Phys.* **1979**, *12* (24), 5361–5369. https://doi.org/10.1088/0022-3719/12/24/008.

(16) Funnell, N. P.; Dove, M. T.; Goodwin, A. L.; Parsons, S.; Tucker, M. G. Local Structure Correlations in Plastic Cyclohexane - A Reverse Monte Carlo Study. *J. Phys. Condens. Matter* **2013**, *25*. https://doi.org/10.1088/0953-8984/25/45/454204.

(17) Fabini, D. H.; Siaw, T. A.; Stoumpos, C. C.; Laurita, G.; Olds, D.; Page, K.; Hu, J. G.; Kanatzidis, M. G.; Han, S.; Seshadri, R. Universal Dynamics of Molecular Reorientation in Hybrid Lead Iodide Perovskites. *J. Am. Chem. Soc.* **2017**, *139*, 16875–16884. https://doi.org/10.1021/jacs.7b09536.

(18) Beecher, A. N.; Semonin, O. E.; Skelton, J. M.; Frost, J. M.; Terban, M. W.; Zhai, H.; Alatas, A.; Owen, J. S.; Walsh, A.; Billinge, S. J. L. Direct Observation of Dynamic Symmetry Breaking above Room Temperature in Methylammonium Lead Iodide Perovskite. *ACS Energy Lett.* **2016**, *1*, 880–887. https://doi.org/10.1021/acsenergylett.6b00381.

(19) Aeberhard, P. C.; Refson, K.; David, W. I. F. Molecular Dynamics Investigation of the Disordered Crystal Structure of Hexagonal $LiBH_4$. *Phys. Chem. Chem. Phys.* **2013**, *15*, 8081. https://doi.org/10.1039/c3cp44520h.

(20) Skripov, A. V.; Babanova, O. A.; Soloninin, A. V.; Stavila, V.; Verdal, N.; Udovic, T. J.; Rush, J. J. Nuclear Magnetic Resonance Study of Atomic Motion in $A_2B_{12}H_{12}$ (A = Na, K, Rb, Cs): Anion Reorientations and Na^+ Mobility. *J. Phys. Chem. C* **2013**, *117*, 25961–25968. https://doi.org/10.1021/jp4106585.

(21) Soloninin, A. V; Dimitrievska, M.; Skoryunov, R. V; Babanova, O. A.; Skripov, A. V; Tang, W. S.; Stavila, V.; Orimo, S. I.; Udovic, T. J. Comparison of Anion Reorientational Dynamics in MCB_9H_{10} and $M_2B_{10}H_{10}$ (M = Li, Na) via Nuclear Magnetic Resonance and Quasielastic Neutron Scattering Studies. *J Solid State Chem C* **2017**, *121*, 1000–1012. https://doi.org/10.1021/acs.jpcc.6b09113.

(22) Tang, W. S.; Unemoto, A.; Zhou, W.; Stavila, V.; Matsuo, M.; Wu, H.; Orimo, S. I.; Udovic, T. J. Unparalleled Lithium and Sodium Superionic Conduction in Solid Electrolytes with Large Monovalent Cage-like Anions. *Energy Environ. Sci.* **2015**, *8*, 3637–3645. https://doi.org/10.1039/c5ee02941d.

(23) Skripov, A. V; Skoryunov, R. V; Soloninin, A. V; Babanova, O. A.; Tang, W. S.; Stavila, V.; Udovic, T. J. Anion Reorientations and Cation Diffusion in $LiCB_{11}H_{12}$ and $NaCB_{11}H_{12}$: ^{1}H, ^{7}Li, and ^{23}Na NMR Studies. *J Solid State Chem C* **2015**, *119*, 26912–26918. https://doi.org/10.1021/acs.jpcc.5b10055.

(24) Soper, A. K.; Barney, E. R. Extracting the Pair Distribution Function from White-Beam X-Ray Total Scattering Data. *J. Appl. Crystallogr.* **2011**, *44*, 714–726. https://doi.org/10.1107/S0021889811021455.

(25) Keen, D. A. A Comparison of Various Commonly Used Correlation Functions for Describing Total Scattering. *J. Appl. Crystallogr.* **2001**, *34*, 172–177. https://doi.org/10.1107/S0021889800019993.

(26) Farrow, C. L.; Juhas, P.; Liu, J. W.; Bryndin, D.; Boin, E. S.; Bloch, J.; Proffen, T.; Billinge, S. J. L. PDFfit2 and PDFgui: Computer Programs for Studying Nanostructure in Crystals. *J. Phys. Condens. Matter* **2007**, *19* (33), 335219. https://doi.org/10.1088/0953-8984/19/33/335219.

(27) Coelho, A. A. TOPAS and TOPAS-Academic: An Optimization Program Integrating Computer Algebra and Crystallographic Objects Written in C++: An. *J. Appl. Crystallogr.* **2018**, *51*, 210–218. https://doi.org/10.1107/S1600576718000183.

(28) Terban, M. W.; Billinge, S. J. L. Structural Analysis of Molecular Materials Using the Pair Distribution Function. *Chem. Rev.* **2022**, *122*, 1208–1272. https://doi.org/10.1021/acs.chemrev.1c00237.

(29) Callear, S. K.; Anne Nickels, E.; Jones, M. O.; Matsuo, M.; Orimo, S. I.; Edwards, P. P.; David, W. I. F. Order and Disorder in Lithium Tetrahydroborate. *J. Mater. Sci.*

2011, *46*, 566–569. https://doi.org/10.1007/s10853-010-5024-0.

(30) Jeong, I. K.; Heffner, R. H.; Graf, M. J.; Billinge, S. J. L. Lattice Dynamics and Correlated Atomic Motion from the Atomic Pair Distribution Function. *Phys. Rev. B* **2003**, *67*, 104301. https://doi.org/10.1103/PhysRevB.67.104301.

(31) Prill, D.; Juhás, P.; Schmidt, M. U.; Billinge, S. J. L. Modelling Pair Distribution Functions (PDFs) of Organic Compounds: Describing Both Intra- and Intermolecular Correlation Functions in Calculated PDFs. *J. Appl. Crystallogr.* **2015**, *48*, 171–178. https://doi.org/10.1107/S1600576714026454.

(32) Proffen, T.; Billinge, S. J. L.; Egami, T.; Louca, D. Structure Analysis of Complex Materials Using the Atomic Pair Distribution Function. *Z. Kristallogr.* **2003**, *218*, 132–143. https://doi.org/10.1524/zkri.218.2.132.20664.

(33) Johnson, R. D.; Yannoni, C. S.; Dorn, H. C.; Salem, J. R.; Bethune, D. S. C_{60} Rotation in the Solid State: Dynamics of a Faceted Spherical Top. *Science* **1992**, *255*, 1235–1238. https://doi.org/10.1126/science.255.5049.1235.

(34) Tang, W. S.; Yoshida, K.; Soloninin, A. V.; Skoryunov, R. V.; Babanova, O. A.; Skripov, A. V.; Dimitrievska, M.; Stavila, V.; Orimo, S. I.; Udovic, T. J. Stabilizing Superionic-Conducting Structures via Mixed-Anion Solid Solutions of Monocarba-Closo-Borate Salts. *ACS Energy Lett.* **2016**, *1* (4), 659–664. https://doi.org/10.1021/acsenergylett.6b00310.

(35) Schlem, R.; Burmeister, C. F.; Michalowski, P.; Ohno, S.; Dewald, G. F.; Kwade, A.; Zeier, W. G. Energy Storage Materials for Solid-State Batteries: Design by Mechanochemistry. *Adv. Energy Mater.* **2021**, *11*, 2101022. https://doi.org/10.1002/aenm.202101022.

(36) Pringle, J. M. Recent Progress in the Development and Use of Organic Ionic Plastic Crystal Electrolytes. *Phys. Chem. Chem. Phys.* **2013**, *15*, 1339–1351.

(37) Timmermans, J. Plastic Crystals: A Historical Review. *J. Phys. Chem. Solids* **1961**, *18*, 1–8. https://doi.org/10.1016/0022-3697(61)90076-2.

(38) Narten, A. H.; Thiessen, W. E.; Blum, L. Atom Pair Distribution Functions of Liquid Water at 25°C from Neutron Diffraction. *Science* **1982**, *217*, 1033–1034. https://doi.org/10.1126/science.217.4564.1033.

(39) Ding, J.; Xu, M.; Guan, P. F.; Deng, S. W.; Cheng, Y. Q.; Ma, E. Temperature Effects on Atomic Pair Distribution Functions of Melts. *J. Chem. Phys.* **2014**, *140*, 064501. https://doi.org/10.1063/1.4864106.

(40) Famprikis, T.; Bouyanfif, H.; Canepa, P.; Zbiri, M.; Dawson, J. A.; Suard, E.; Fauth, F.; Playford, H. Y.; Dambournet, D.; Borkiewicz, O. J.; et al Insights into the Rich Polymorphism of the Na^+Ion Conductor Na_3PS_4 from the Perspective of Variable-Temperature Diffraction and Spectroscopy. *Chem. Mater.* **2021**, *33*, 5652–5667. https://doi.org/10.1021/acs.chemmater.1c01113.

(41) Scholz, T.; Schneider, C.; Terban, M. W.; Deng, Z.; Eger, R.; Etter, M.; Dinnebier, R. E.; Canepa, P.; Lotsch, B. V. Superionic Conduction in the Plastic Crystal Polymorph of $Na_4P_2S_6$. *ACS Energy Lett.* **2022**, *7*, 1403–1411. https://doi.org/10.1021/acsenergylett.1c02815.

TOC Graphic

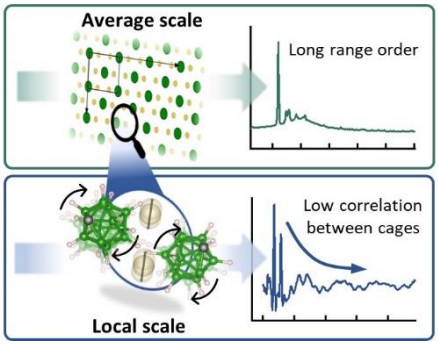
Average scale
Long range order
Low correlation
between cages
Local scale